UNIVERSIDAD DISTRITAL
FRANCISCO JOSÉ DE CALDAS

Ingeniería

https://revistas.udistrital.edu.co/index.php/reving/issue/view/1291

DOI: https://doi.org/10.14483/23448393.22926

Research

Theoretical-Experimental Modal Analysis of a Flexible Rotor Based on the Jeffcott Model

Análisis modal teórico-experimental de un rotor flexible basado en el modelo de Jeffcott

Javier Hernando Ruíz-Rodríguez[1,2]*, Brian Farid Morales-Hernández[1,2], and Heller Guillermo Sánchez-Acevedo[1]

[1]Research Group on Energy and Environment (GIEMA), Department of Mechanical Engineering, Universidad Industrial de Santander, Bucaramanga, Colombia
[2]Sielecom SAS, Bucaramanga, Colombia

Abstract

Context: Rotating equipment that operates at high speeds or handles significant loads is designed based on the concept of *flexible shafts*. This is the case with turbines, compressors, and turbopumps, among others. The theoretical-experimental modal analysis of these shafts is crucial for ensuring a safe and efficient operation, as well as for identifying appropriate maintenance strategies.

Method: In this work, we perform both theoretical and experimental modal analyses of an isotropic flexible rotor based on the Jeffcott model. The theoretical modal analysis is carried out using a numerical model with conditions similar to those of the experimental analysis. The results are compared using the modal assurance criterion (MAC). The validated numerical model enables the evaluation of eigenfrequencies and their associated modal shapes.

Results: The first two bending natural modes of the flexible rotor were obtained from the theoretical and experimental modal analysis, and the mode shapes and natural frequencies were determined. The mode shapes were correlated, exhibiting a correlation value greater than 88 %, thus validating the numerical model.

Conclusions: This approach not only enhances the understanding of the shaft's dynamic response but also contributes to improved decision-making during the design and operation stages of rotating systems in various industrial applications.

Keywords: experimental modal analysis, theoretical modal analysis, natural frequencies, MAC, vibration mode shapes, flexible rotors, Jeffcott rotor.

Article history

Received: Nov 21st, 2024

Modified: May 15th, 2025

Accepted: June 20th, 2025

Ing, vol. 30, no. 2, 2025, e22926

*Correspondence: javier2228057@correo.uis.edu.co, bmorales@sielecom.com

Resumen

Contexto: El equipo rotativo que opera a altas velocidades o maneja cargas significativas se diseña con base en el concepto de *ejes flexibles*. Este es el caso de las turbinas, los compresores y las turbobombas, entre otros. El análisis modal teórico-experimental de estos ejes es esencial para garantizar una operación segura y eficiente, así como para identificar estrategias de mantenimiento adecuadas.
Método: En este trabajo desarrollamos análisis modales tanto teóricos como experimentales de un rotor flexible isotrópico basado en el modelo de Jeffcott. El análisis modal teórico se realiza utilizando un modelo numérico con condiciones similares a las del análisis experimental. Los resultados se comparan utilizando el criterio de aseguramiento modal (MAC). El modelo numérico validado permite evaluar las frecuencias propias y sus formas modales asociadas.
Resultados: Se obtuvieron los dos primeros modos naturales de flexión del rotor flexible del análisis modal teórico y experimental, y se determinaron las formas modales y las frecuencias naturales. Las formas modales estuvieron correlacionadas, obteniendo un valor de correlación superior al 88 %, lo que valida el modelo numérico.
Conclusiones: Este enfoque no solo mejora la comprensión de la respuesta dinámica del eje, sino que también contribuye a mejorar la toma de decisiones durante las etapas de diseño y operación de sistemas rotativos en diversas aplicaciones industriales.

Palabras clave: análisis modal experimental, análisis modal teórico, frecuencias naturales, MAC, modos de vibración, rotores flexibles, rotor de Jeffcott.

Table of contents

1. Introduction

Rotating machines operating at high speeds and loads, such as turbines, compressors, and turbopumps, are typically designed with flexible shafts (1). Analyzing the natural frequencies and mode shapes of these systems is essential for ensuring their safe and efficient operation. Theoretical and experimental modal analyses have become key tools for identifying critical speeds and defining appropriate maintenance strategies (2, 3).

This work conducts a theoretical and experimental modal analysis on a Jeffcott-based rotor. A numerical model based on the finite element method (FEM) is used to simulate the rotor's conditions, and the results are compared against experimental data using the modal assurance criterion (MAC). This criterion facilitates the validation of the numerical model by assessing its consistency with the rotor's dynamic behavior.

The application of theoretical and experimental modal analysis to rotors has been an active research area in structural and mechanical dynamics, particularly in rotating machinery (4–6). Due to its simplicity and its ability to represent the dynamic behavior of more complex systems, the Jeffcott rotor (7) has been widely used in similar studies to analyze the vibration responses of rotating systems (8). Several studies have developed numerical models to simulate the behavior of its shafts under varying load and rotational speed conditions (9, 10). In recent years, simulation tools such as the FEM have enabled a precise analysis of the dynamic behavior of flexible shafts (11). These tools make it possible to accurately determine natural frequencies and mode shapes, which is essential for avoiding resonance issues during the operation of rotating machinery (9). Additionally, advancements in sensors and excitation systems (*e.g.*, shakers) have significantly improved the quality of the results obtained through experimental modal analysis.

Numerical modal validation requires the comparison of numerical results against experimental data (5, 12). In this context, experimental modal analysis (EMA) is a highly useful tool. EMA is a test that allows acquiring modal information about an element, including the frequency response to the applied excitation forces (13). Comparing the outcomes of theoretical modal analysis (TMA) against those of EMA allows validating numerical results, ensuring an adequate correlation between the vibration mode shapes obtained in both analyses. This approach has led to a better understanding of the behavior of rotating systems, contributing to improved design and maintenance strategies for industrial equipment.

In addition to classical approaches to rotor modeling and experimental validation, several studies have addressed more advanced rotor systems using nonlinear dynamics and active control strategies. For instance, (14) investigated the whirling behavior and rub/impact phenomena of a 16-pole rotor supported by active magnetic bearings (AMBs), employing the multiple scales method to analyze the system's nonlinear response. More recently, (15) proposed a tuned positive position feedback (TPPF) control strategy to mitigate vibrations in a magnetically suspended rotor, demonstrating the effectiveness of control design in stabilizing rotor motion under various conditions. Although these studies focus on AMB- supported systems, they provide valuable insights into rotor dynamics beyond the scope of linear free-free configurations.

This research was conducted in three stages: 1) numerical model implementation, 2) experimental modal analysis, and 3) model validation using the MAC. The numerical model of the rotor was developed based on the FEM. The process began by selecting the coordinate system and defining the degrees of freedom. Next, the type and number of elements for the rotor were discretized to strike a balance between accuracy and computational cost. Through this discretization, the mass and stiffness matrices were assembled to describe the system's dynamic behavior. Subsequently, the eigenvalue problem was solved to numerically obtain the rotor's natural frequencies and mode shapes. Following this, EMA was carried out. Multiple equidistant points were marked on the rotor, which was suspended by elastics to simulate free-free boundary conditions. An accelerometer was placed at a reference point, and each marked point was impacted with a hammer. These measurements were used to calculate the frequency response functions, from which modal identification was performed. Finally, the rotor's

numerical model was validated by correlating the results of the experimental and numerical modal analyses. The degree of similarity between modes was determined using the MAC, which quantifies the agreement between experimental and numerical mode shapes (16).

2. Numerical model

The rotor analyzed in both the numerical and experimental studies consisted of a steel shaft with a centrally mounted aluminum disk. This simple and symmetric configuration is representative of the basic rotor geometries that are often used in rotordynamic studies, and it allows for a clear identification of bending modes and natural frequencies. The geometric dimensions and material properties of both components are summarized in Table **I**.

Table I. Geometric dimensions and mechanical properties of the shaft and disk

Component	Material	Diameter (cm)	Length/thickness (cm)	Modulus of elasticity (GPa)	Density (Kg/m^3)
Shaft	AISI 4140 steel	1.15	31.7	205	7850
Disk	Aluminum	9.44	2.5	70	2700

The numerical model was implemented and solved in the MATLAB programming environment. This formulation is based on the equation of motion for a forced system (17), which governs the rotor's dynamic behavior and is expressed in matrix form, as shown in Eq. (1).

$$\mathbf{M\ddot{q}} + \mathbf{C\dot{q}} + \mathbf{Kq} = \mathbf{f} \tag{1}$$

where M represents the mass matrix, C the damping matrix, K the stiffness matrix, f the force vector, q the displacement vector, $\dot{q}$ the velocity vector, and $\ddot{q}$ the acceleration vector. To study the free vibrations of the Jeffcott rotor, damping is neglected, and the external force is set to zero. The resulting equation is known as the *equation of motion for a free system* (18, 19) and is presented in Eq. (2).

$$\mathbf{M\ddot{q}} + \mathbf{Kq} = 0 \tag{2}$$

Using the defined equation of motion, the shaft is discretized into eight linear beam elements, each consisting of two nodes and eight degrees of freedom (DOF), four per node, two translational (v and ϑ) and two rotational (θ and ϕ). Axial DOF are not considered, as this study focuses on lateral vibrations. Fig. **1** illustrates the reference coordinates and the associated DOF.

Based on the rotor discretization, the element mass matrix M_e and the stiffness matrix K_e for each rotor element are computed using the energy method and Euler-Bernoulli beam theory. This formulation neglects both rotary inertia and shear deformation, which is appropriate for the slender shaft geometry considered in this work (5, 20, 21). The resulting matrices are shown in Eqs. (3) and (4). Afterwards, the

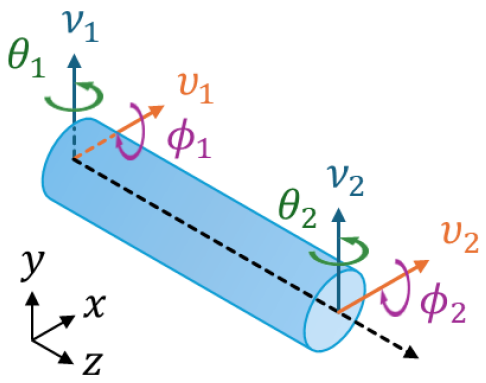

Figure 1. DOFs and reference coordinates

element matrices are assembled according to their corresponding DOF, yielding the global mass M and stiffness K matrices.

$$\mathbf{M}_e = \frac{AL_e\rho}{420}\begin{bmatrix} 156 & 0 & 0 & 22L_e & 54 & 0 & 0 & -13L_e \\ 0 & 156 & -22L_e & 0 & 0 & 54 & 13L_e & 0 \\ 0 & -22L_e & 4L_e^2 & 0 & 0 & -13L_e & -3L_e^2 & 0 \\ 22L_e & 0 & 0 & 4L_e^2 & 13L_e & 0 & 0 & -3L_e^2 \\ 54 & 0 & 0 & 13L_e & 156 & 0 & 0 & -22L_e \\ 0 & 54 & -13L_e & 0 & 0 & 156 & 22L_e & 0 \\ 0 & 13L_e & -3L_e^2 & 0 & 0 & 22L_e & 4L_e^2 & 0 \\ -13L_e & 0 & 0 & -3L_e^2 & -22L_e & 0 & 0 & 4L_e^2 \end{bmatrix} \tag{3}$$

$$\mathbf{K}_e = \frac{EI}{L_e^3}\begin{bmatrix} 12 & 0 & 0 & 6L_e & -12 & 0 & 0 & 6L_e \\ 0 & 12 & -6L_e & 0 & 0 & -12 & -6L_e & 0 \\ 0 & -6L_e & 4L_e^2 & 0 & 0 & 6L_e & 2L_e^2 & 0 \\ 6L_e & 0 & 0 & 4L_e^2 & -6L_e & 0 & 0 & 2L_e^2 \\ -12 & 0 & 0 & -6L_e & 12 & 0 & 0 & -6L_e \\ 0 & -12 & 6L_e & 0 & 0 & 12 & 6L_e & 0 \\ 0 & -6L_e & 2L_e^2 & 0 & 0 & 6L_e & 4L_e^2 & 0 \\ 6L_e & 0 & 0 & 2L_e^2 & -6L_e & 0 & 0 & 4L_e^2 \end{bmatrix} \tag{4}$$

where A denotes the cross-sectional area, L_e the length of the element, ρ the material density, E the modulus of elasticity, and I the element's second moment of inertia. The mass contribution of the disk is incorporated into the overall mass matrix as a concentrated (or point) mass (22) at the disk's location node – specifically at node 5. The disk mass matrix is presented in Eq. (5).

$$\mathbf{M}_d = \begin{bmatrix} m_d & 0 & 0 & 0 \\ 0 & m_d & 0 & 0 \\ 0 & 0 & J_d & 0 \\ 0 & 0 & 0 & J_d \end{bmatrix} \tag{5}$$

where m_d is the mass of the disk and J_d is the moment of inertia of the disk perpendicular to the axis of rotation. With the global mass matrix M and stiffness matrix K established, the eigenvalue and

eigenvector problem is solved as shown in Eq. (6).

$$\mathbf{M}^{-1}\mathbf{K}\mathbf{x} = \lambda\mathbf{x} \tag{6}$$

where $\mathbf{x}$ represents the eigenvectors of the system associated with the mode shapes, and λ represents the eigenvalues, which are related to the natural frequencies ω_n, as shown in Eq. (7). In this work, the eigenvalue problem was solved using MATLAB's *eig* function.

$$\lambda = \omega_n^2 \tag{7}$$

3. Experimental modal analysis

To conduct the EMA, the shaft was divided into eight equidistant segments, resulting in nine measurement positions (Fig. 2). The selection of measurement and excitation points was based on a preliminary numerical modal analysis (NMA) of the first two bending modes. From this analysis, point 6 was chosen as the reference accelerometer position, as it corresponds to an antinode and avoids nodes, thus ensuring an effective capture of the response. All nine positions were used as points for excitation with the impact hammer, in order to ensure an adequate modal coverage.

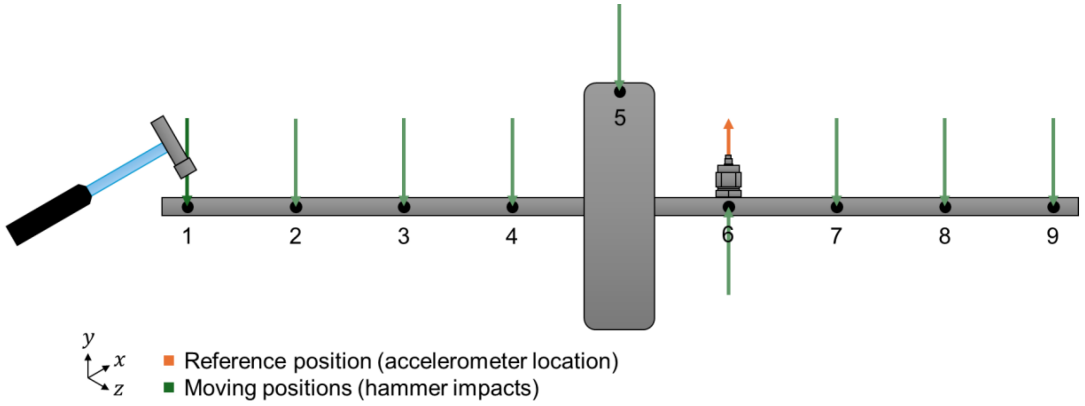

Figure 2. Configuration of the EMA measurement setup

It should be noted that this type of experimental test requires specific planning for each rotor configuration. The location of the accelerometers, excitation points, and frequency range must consider prior numerical simulations and the specific geometric and dynamic characteristics of the rotor under study. In this case, the shaft was suspended using elastic bands to approximate free-free boundary conditions (Fig. 3).

Additionally, Fig. 4 presents the data acquisition system used for the test, including the measurement software interface and the vibration analyzer equipment.

The equipment and instrumentation used for the EMA, along with their main specifications, are listed in Table II.

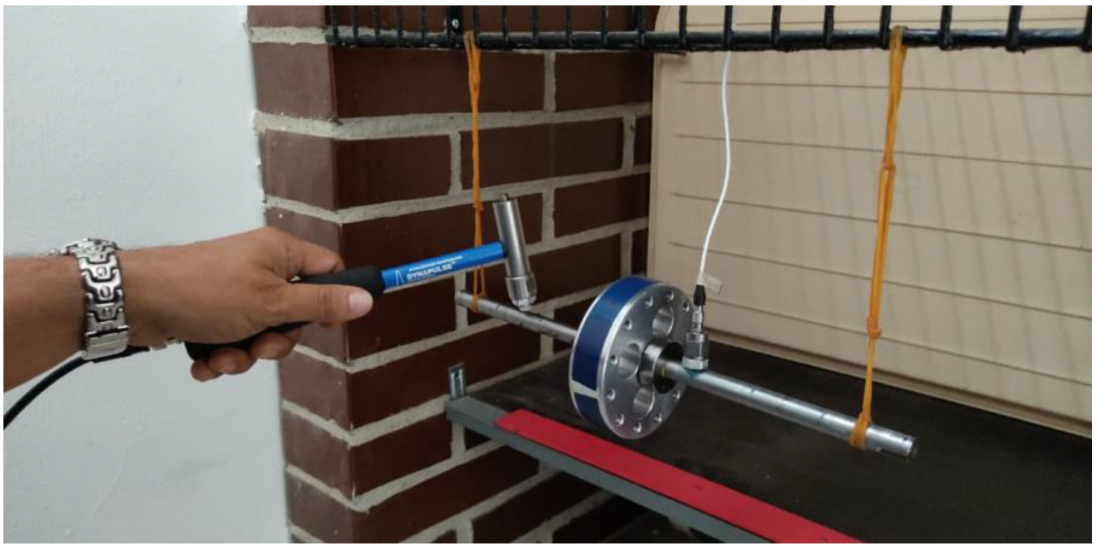

Figure 3. Experimental setup showing the suspended shaft, accelerometer, and impact hammer for simulating free-free boundary conditions

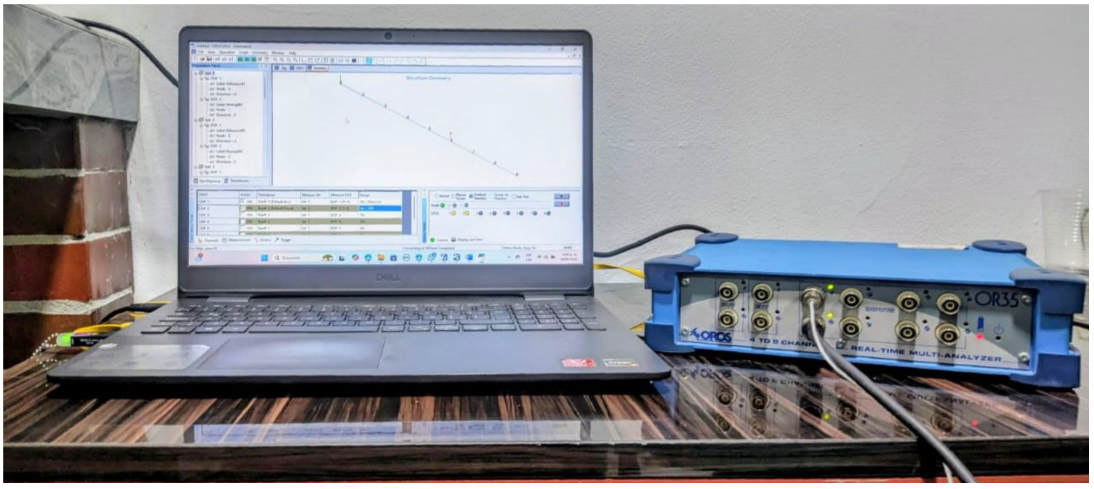

Figure 4. Data acquisition system used in the experimental tests, including the software interface and vibration analyzer

Table II. General specifications of the equipment and instruments used in the EMA

Equipment or instrument	Specifications
OROS OR35 analyzer	Up to 102.4 KS/s
Dytran 3056B1 uniaxial accelerometer	Sensitivity: 10mV/g
Dytran 5800B5 hammer	Sensitivity: 4.83 mV/lbf

The OROS modal software was used to acquire and process data, as well as to perform the EMA. The main configuration parameters related to the acquisition and processing of the response and excitation force signals are shown in Table III.

Table III. Configuration parameters for the EMA in the OROS modal software

Parameter	Value
Frequency range	0-2000 Hz
Spectral lines	801
Sampling time	400 ms
% overlap	67
Type of averaging	Linear
Number of averages	3
Window type	Force/Exp

The modal characteristics were calculated from the frequency response functions (FRF) over the entire measurement range. This was done using the broadband method, which employs a robust modal identification algorithm. To apply this method, a frequency range of 167.5-1125 Hz was selected from the modal indication function (MIF) plot. This selection was made by identifying the most prominent peaks and adjusting the limits to the troughs at the beginning of the first peak and at the end of the last peak of interest (Fig. 5).

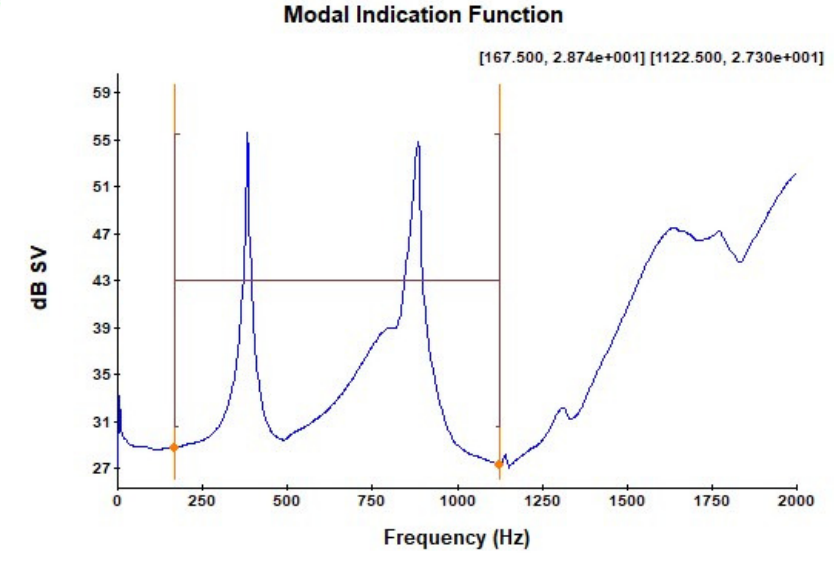

Figure 5. MIF of the EMA of the rotor

Once the frequency range had been established, modal identification began by obtaining the poles from the stabilization diagram (Fig. 6). The poles were determined by defining two preset modes, a minimum of 16 modes, and a range of 12 modes. The two frequencies that showed the greatest

coincidence with the peaks of the MIF and the frequencies of the stable poles, identified by the green s in the stabilization diagram, were selected.

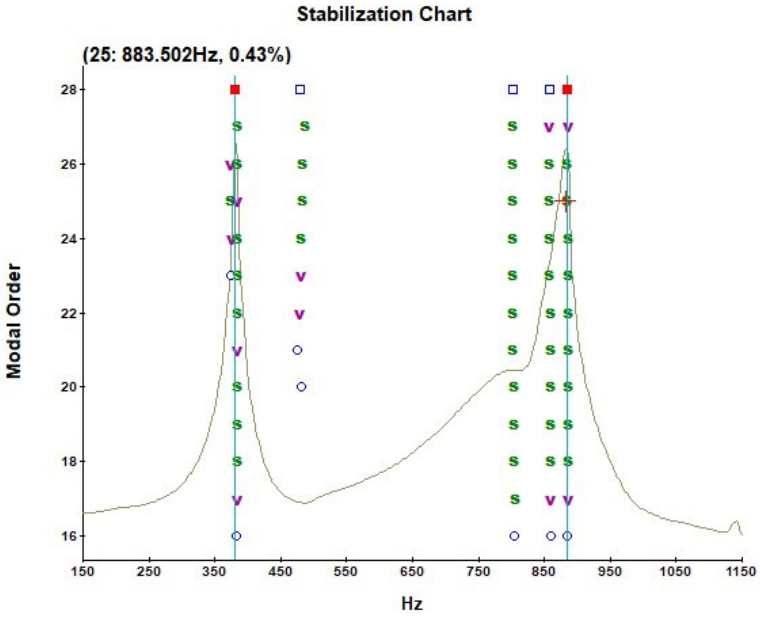

Figure 6. Mode stabilization chart

With the selected frequencies, the deflection shapes were calculated, and the synthesized frequency response function (SFRF) was obtained (Fig. 7). The graph shows the fit, regarding both peak location and phase, of the selected eigenfrequencies between the synthesized FRF and the frequency response function obtained from the measurements.

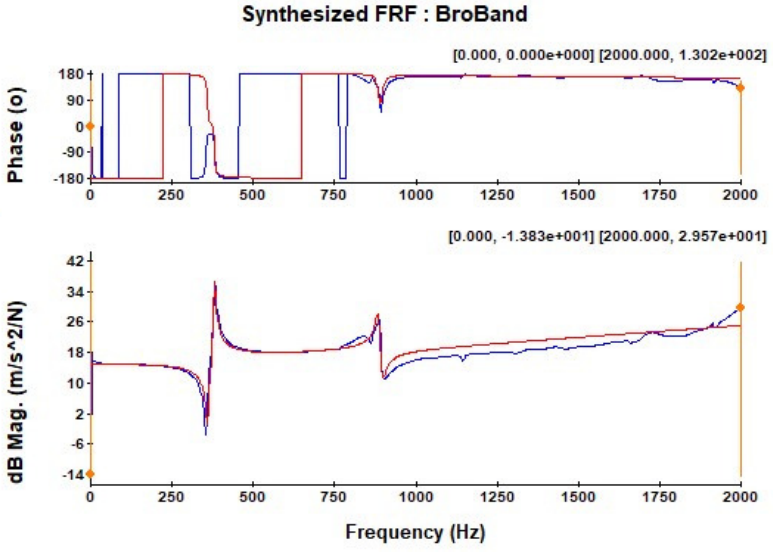

Figure 7. Frequency response function synthesized using the broadband method

4. Model validation

The numerical model was validated using the MAC. This method correlates the modes obtained from two different sources (numerical-numerical, numerical-experimental, or experimental-experimental). The MAC value indicates the degree of correlation and correspondence between the two sets of modes. It ranges from 0 to 1, with a value of 1 representing the highest degree of correlation between the modes. The MAC (16) is defined in Eq. (8).

$$\mathbf{MAC}_{xai} = \frac{\left|\boldsymbol{\psi}_{xi}^{T}\boldsymbol{\psi}_{ai}\right|^{2}}{\left(\boldsymbol{\psi}_{xi}^{T}\boldsymbol{\psi}_{xi}\right)\left(\boldsymbol{\psi}_{ai}^{T}\boldsymbol{\psi}_{ai}\right)} \tag{8}$$

where ψ_x is the experimental modal vector, and ψ_a is the numerical modal vector for mode i. The superscript T denotes the conjugate transpose of the modal vector.

5. Results analysis

The deflection shapes (or modal shapes) obtained from the numerical model exhibit the typical morphological characteristics of bending modes. Specifically, the first mode shows two nodes and three antinodes, while the second mode has three nodes and four antinodes. The frequencies associated with these modes are 368.7 and 841 Hz, respectively, which confirm the rotor's ability to operate across a wide range of speeds. The modal shapes, along with the natural frequencies corresponding to the first two bending modes of the rotor, are shown in Fig. 8, as obtained from the implemented numerical model.

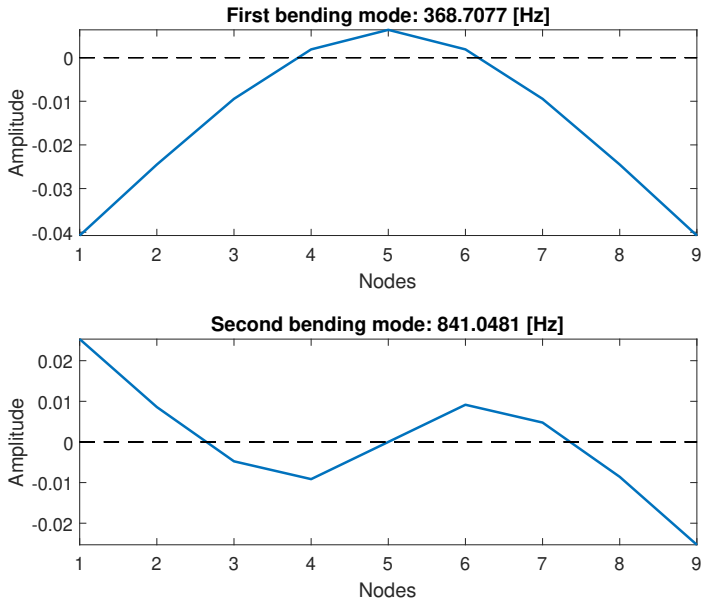

Figure 8. First and second rotor bending modes obtained from the numerical model

The modal shapes obtained from the EMA reveal one mode corresponding to the first rotor bending mode and another associated with the second bending mode. The natural frequencies associated with these modes are 381.2 and 883.85 Hz. Based on these results, the rotor's safe operating speed range is limited to approximately 0-18,300 RPM, *i.e.*, 20 % below the first bending natural frequency. This prevents the rotor from operating near the critical speed. The deflection of the first two modes shows a slight asymmetry at the ends, which may be caused by changes in stiffness and mass in the area where the keyseat or wedge is located (on the left side of the rotor). The experimental modal shapes and their natural frequencies are shown in Fig. 9.

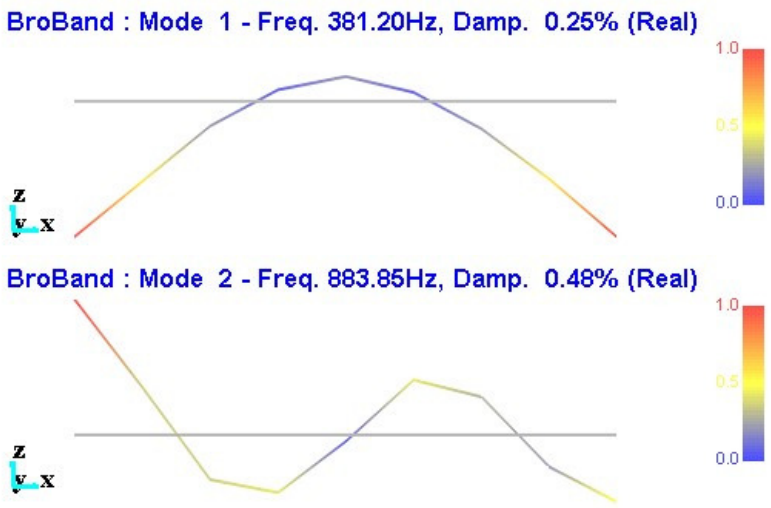

Figure 9. First and second rotor bending modes obtained from the EMA

The results of applying the MAC show a high degree of correlation and correspondence between the modes obtained from the EMA and those from the numerical model. The first bending mode shows a 99.78 % correlation, while the second bending mode exhibits an 88.66 % correlation. These correlation and correspondence values validate the implemented numerical model. The results of the MAC application are shown in Fig. 10.

While updating the active magnetic bearing rotor model, (23) used the MAC as part of the updating function. The values obtained were close to 1, exceeding 97.9 % and approaching 100 % for the first modes. The higher correlation of mode shapes compared to our results can be attributed to the larger number of nodes in the EMA and the greater number of DOF in the numerical model, along with the precision of the material's mechanical properties defined in the numerical model.

6. Conclusions

According to the MAC method, the numerical model of the rotor shows a correlation and agreement of over 88 % with the results from the EMA for the analyzed bending natural frequencies. These results validate the implemented model.

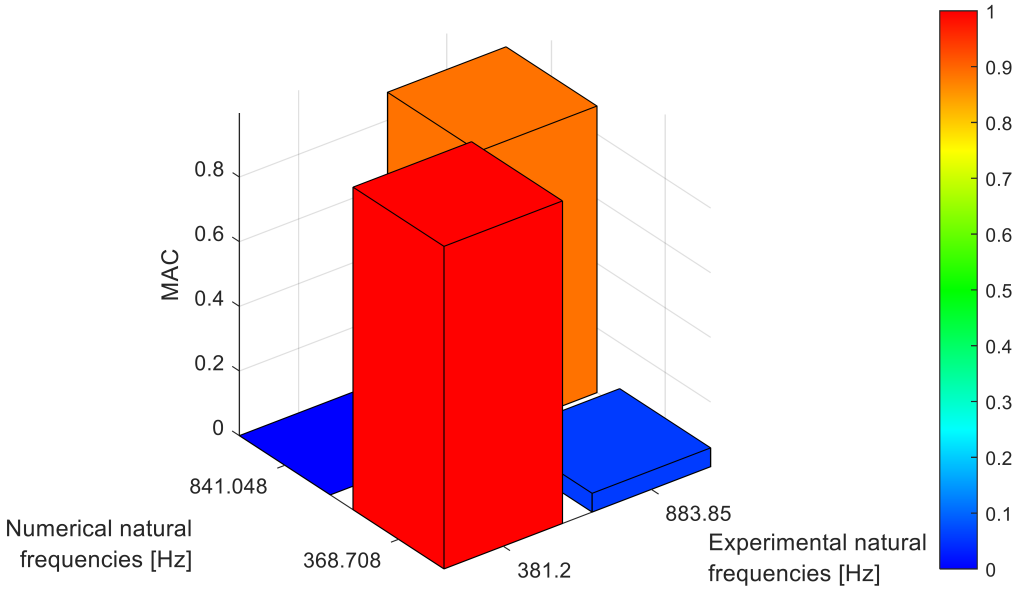

Figure 10. MAC between the experimental and numerical rotor modes

The first two bending modes of the shaft have natural frequencies of 381.2 and 883.85 Hz, and their deflection shapes exhibit the typical morphological characteristics of this type of shaft or beam. The relatively high values of the natural frequencies allow the shaft to operate across a wide speed range, up to 18,297 rpm, ensuring that the shaft operates below 20 % of the first natural bending frequency.

The use of linear beam elements facilitates the implementation of the rotor's numerical model, given their ability to adapt to the geometry and behavior of the shafts, offering an optimal balance between accuracy and computational efficiency. This allows simulating the dynamic behavior of rotating structures, such as flexible shafts, at a relatively low computational cost.

7. CRediT author statement

Javier Hernando Ruiz-Rodríguez. Conceptualization, methodology, investigation, writing (original draft), data curation, project administration, and funding acquisition.
Brian Farid Morales-Hernández. Conceptualization, methodology, investigation, writing (original draft, review & editing), visualization, software, data curation, formal analysis, and validation.
Heller Guillermo Sánchez-Acevedo. Investigation, supervision, writing (review & editing), and project administration.

References

[1] H. G. Sánchez-Acevedo, "Modelo analítico para el estudio de la torsión en rotores flexibles," *Rev. UIS Ing.*, vol. 9, no. 1, pp. 69–76, 2010. ↑2

[2] V. Gagnol, T.-P. Le, and P. Ray, "Numerical and experimental high speed machining spindle-tool modal characterization (dynamics of machine components)," in *Proc. Asian Conf. Multibody Dyna.*, 2010, pp. 57636-1–57636-11. https://doi.org/10.1299/jsmeacmd.2010.5._57636-1 ↑2

[3] Z. Huang and B. Han, "Effective approach for calculating critical speeds of high-speed permanent magnet motor rotor-shaft assemblies," *IET Electr. Power Appl.*, vol. 9, no. 9, pp. 628–633, Nov. 2015. https://doi.org/10.1049/iet-epa.2014.0503 ↑2

[4] H. G. Sánchez, F. R. Nova, and O. A. González-Estrada, "Implementation of the operational modal analysis technique in a power transmission shaft," *J. Phys. Conf. Ser.*, vol. 1247, no. 1, art. 012032, Jun. 2019. https://doi.org/10.1088/1742-6596/1247/1/012032 ↑3

[5] B. F. Morales-Hernández, "Metodología para el ajuste y validación del modelo numérico de un rotor de Jeffcott, mediante el uso de funciones de respuesta en frecuencia (FRF)," Master's thesis, Universidad Industrial de Santander, Bucaramanga, Colombia, 2023. ↑3, 4

[6] Z. Huang, B. Han, and Y. Le, "Modeling method of the modal analysis for turbomolecular pump rotor blades," *Vacuum*, vol. 144, pp. 145–151, Oct. 2017. https://doi.org/10.1016/j.vacuum.2017.07.029 ↑3

[7] H. H. Jeffcott, "The lateral vibration of loaded shafts in the neighbourhood of a whirling speed.—The effect of want of balance," *Lond. Dub. Edim. Phil. Mag. J. Sci.*, vol. 37, pp. 304–314, 1919. https://doi.org/10.1080/14786440308635889 ↑3

[8] A. Malgol, K. P. Vineesh, and A. Saha, "Investigation of vibration characteristics of a Jeffcott rotor system under the influence of nonlinear restoring force, hydrodynamic effect, and gyroscopic effect," *J. Brazilian Soc, Mech. Sci. Eng.*, vol. 44, no. 3, p. 105, 2022. https://doi.org/10.1007/s40430-021-03277-x ↑3

[9] J. Liu, C. Tang, and G. Pan, "Dynamic modeling and simulation of a flexible-rotor ball bearing system," *J. Vibr. Control*, vol. 28, no. 23–24, pp. 3495–3509, Dec. 2022. https://doi.org/10.1177/10775463211034347 ↑3

[10] A. Blanco-Ortega, F. Beltrán-Carbajal, G. Silva-Navarro, and H. Méndez-Azúa, "Control de vibraciones en maquinaria rotatoria," *Rev. Ibero. Autom, Infor, Ind. RIAI*, vol. 7, no. 4, pp. 36–43, Oct. 2010. https://doi.org/10.1016/s1697-7912(10)70058-3 ↑3

[11] E. Sarrouy, O. Dessombz, and J.-J. Sinou, "Stochastic analysis of the eigenvalue problem for mechanical systems using polynomial chaos expansion— Application to a finite element rotor," *J. Vibr. Acoust.*, vol. 134, no. 5, art. 051009, Oct. 2012. https://doi.org/10.1115/1.4005842 ↑3

[12] J. Páez Chávez, V. Vaziri Hamaneh, and M. Wiercigroch, "Modelling and experimental verification of an asymmetric Jeffcott rotor with radial clearance," *J. Sound Vibr.*, vol. 334, pp. 86–97, Jan. 2015. https://doi.org/10.1016/j.jsv.2014.05.049 ↑3

[13] Y. M. Ameen and J. K. Ali, "Theoretical and experimental modal analysis of circular cross- section shaft," *IOP Conf. Ser. Mater. Sci. Eng.*, vol. 745, no. 1, art. 012066, Feb. 2020. https://doi.org/10.1088/1757-899X/745/1/012066 ↑3

[14] A. Kandil, "Investigation of the whirling motion and rub/impact occurrence in a 16-pole rotor active magnetic bearings system with constant stiffness," *Nonlinear Dyna.*, vol. 102, no. 4, pp. 2247–2265, Dec. 2020. https://doi.org/10.1007/s11071-020-06071-x ↑3

[15] A. Kandil and Y. S. Hamed, "Tuned positive position feedback control of an active magnetic bearings system with 16-poles and constant stiffness," *IEEE Access*, vol. 9, pp. 73857–73872, 2021. https://doi.org/10.1109/ACCESS.2021.3080457 ↑3

[16] R. J. Allemang, "The modal assurance criterion–Twenty years of use and abuse," *Sound Vibr.*, vol. 37, pp. 14–23, 2003. https://www.sandv.com/downloads/0308alle.pdf ↑4, 10

[17] C. Chen, P. Duffour, and P. Fromme, "Modelling wind turbine tower-rotor interaction through an aerodynamic damping matrix," *J. Sound Vibr.*, vol. 489, art. 115667, Dec. 2020. https://doi.org/10.1016/j.jsv.2020.115667 ↑4

[18] L. Cveticanin, "Free vibration of a Jeffcott rotor with pure cubic non-linear elastic property of the shaft," *Mech. Mach. Theory*, vol. 40, no. 12, pp. 1330–1344, Dec. 2005. https://doi.org/10.1016/j.mechmachtheory.2005.03.002 ↑4

[19] T. H. EL-MAHDY and R. M. GADELRAB, "Free vibration of unidirectional fiber reinforcement composite rotor," *J. Sound Vibr.*, vol. 230, no. 1, pp. 195–202, Feb. 2000. https://doi.org/10.1006/jsvi.1999.2573 ↑4

[20] J. Warminski, L. Kloda, and S. Lenci, "Nonlinear vibrations of an extensional beam with tip mass in slewing motion," *Meccanica*, vol. 55, no. 12, pp. 2311–2335, Dec. 2020. https://doi.org/10.1007/S11012-020-01236-9/TABLES/2 ↑4

[21] J. Taghipour, M. Dardel, and M. H. Pashaei, "Nonlinear vibration mitigation of a flexible rotor shaft carrying a longitudinally dispositioned unbalanced rigid disc," *Nonlinear Dyna.*, vol. 104, no. 3, pp. 2145–2184, May 2021. https://doi.org/10.1007/S11071-021-06428-W/METRICS ↑4

[22] R. Zaradnik, S. Raichman, and A. E. Mirasso, "Comparación de diversas matrices de masas concentradas con similitud de modos propios," *Mecánica Computacional*, vol. 28, no. 10, pp. 853-869. https://www.researchgate.net/publication/329170895_COMPARACION_DE_DIVERSAS_MATRICES_DE_MASAS_CONCENTRADAS_CON_SIMILITUD_DE_MODOS_PROPIOS ↑5

[23] Y. Xu, J. Zhou, L. Di, C. Zhao, and Q. Guo, "Active magnetic bearing rotor model updating using resonance and MAC error," *Shock Vibr.*, vol. 2015, pp. 1–9, 2015. https://doi.org/10.1155/2015/263062 ↑11

Javier Hernando Ruiz-Rodríguez

Electronics engineer from Universidad Antonio Nariño, Master of Science in Reliability and Risk from Universidad de La Gran Canaria. CAT III vibration analyst of the Mobius Institute; CAT II thermograph analyst, PTA; CAT I ultrasound analyst of the Mobius Institute; international instructor of vibrations, CAT I, CAT II, and CAT III; CAT I thermography and CAT I ultrasound, Mobius Institute and Sielecom SAS. Researcher at Sielecom SAS, specialized in mechanical vibrations, rotordynamics, condition monitoring, modal analysis, and numerical model development.

Email: javier2228057@correo.uis.edu.co

Brian Farid Morales-Hernández

Mechanical engineer and Master of Science in Mechanical Engineering from Universidad Industrial de Santander. CAT II vibration analyst of the Mobius Institute. Researcher at Sielecom SAS, focusing on mechanical vibrations, rotordynamics, optimization algorithms, and composite materials.

Email: bmorales@sielecom.com

Heller Guillermo Sánchez-Acevedo

Mechanical engineer with a PhD in Applied and Computational Mechanical Engineering. He has an outstanding track record in the fields of rotordynamics and mechanical vibrations, establishing himself as a reference in his area of expertise. He currently serves as a full professor at the School of Mechanical Engineering of Universidad Industrial de Santander, where he leads the *Mechanical Vibrations* courses of the undergraduate program in Mechanical Engineering and the specialization in Maintenance Management. He is also actively involved in the Master's and PhD programs in Mechanical Engineering, where, in addition to teaching the *Mechanical Vibrations* course, he delivers advanced subjects such as *Rotordynamics* and *Modal Analysis*. His academic work is complemented by a prolific scientific output, reflected in numerous articles published in high-impact journals and the supervision of research projects focused on practical solutions for industrial challenges. Dr. Sánchez has made significant contributions to the industrial sector through the implementation of innovative projects and technical solutions in his field of specialization.

Email: hgsanche@uis.edu.co